International Journal for Housing Science and Its Applications
Publish August 3, 2025. Volume 46, Issue 3 Pages 1108-1119

https://doi.org/10.70517/ijhsa46386

Optimization of Complex Structures and Exploration of Formal Aesthetics in Art Design Empowered by Numerical Computing Methods

Shaoqiang Chen[1,*]
[1] School of Arts and Preschool Education, Henan Logistics Vocational College, Zhengzhou, Henan, 450012, China
Corresponding authors: (e-mail: chen_online@126.com).

Abstract The study systematically explores the synergistic mechanism between complex structural performance enhancement and formal aesthetic expression of topology optimization techniques in art design through numerical computation methods. Based on the homogenization theory and the grid point density method, a macro-micro coupled microstructure topology optimization framework is constructed, combining the quadratic filter and the Heaviside function to realize the structural boundary smoothing, ensuring the unity of mechanical properties and visual fluency. For the complexity of multi-material composite structures, an improved MBESO algorithm is proposed, which balances the performance of tensile and compressive regions by dynamically adjusting the material distribution and stress criterion, and realizes the synergistic optimization of lightweight and aesthetics. Experimental validation shows that the MBESO algorithm reduces the number of iterations to 40 times compared with the traditional BESO, the volume fraction is reduced to 3.3×10-9, and the error of multi-material optimization is less than 7.59%. Through eye tracking and physiological response experiments, it is found that the average gaze time of high-density information-based design is 238.99 ms, which is significantly higher than that of minimalist white space-based design of 205.66 ms, and the emotion-driven design significantly improves the heart rate by 0.387±0.806 bpm, and the change of respiratory rate by 0.906±0.499 resp, which verifies the strong correlation between formal aesthetics and user perception.

Index Terms numerical computing, artistic design, structural topology optimization, homogenization theory, multi-material topology optimization

I. Introduction

Design is a unique human behavior, conscious, inspired, active and resourceful, and the history of mankind is actually a history of continuous design and creation. Design is a tool for human beings to break through physical and mental limitations, transforming the material and spiritual world, providing a realistic basis for the pursuit of various goals, and at the same time, design reconciles the intrinsic and extrinsic values of human beings, and becomes the basis for the realization of various values [1]-[3]. The practical value of art and design is closely related to social life and has obvious direct impact, and other values of art and design also gradually appear and influence social culture [4]. In the context of postmodern art and design aesthetic paradigm expansion, the art structure and formal aesthetics show a pluralistic and metaphorical representation, providing artists and designers with a broader thinking space and richer design topics [5]-[8].

Since entering the industrial society, along with the progress of science and technology and the conflict of traditional humanities, the integration of scientific and technological effects and aesthetic elements of the demand already exists, design aesthetics implies the display of scientific and technological value of the unity of goodness and beauty of the judgment standard [9]-[11]. How to transform scientific and technological values into easily accepted design aesthetics explicit and non-obvious features, and promote the dissemination of scientific and technological values in social life is worth exploring [12], [13]. To this end, numerical computation methods are explored from the unique perspective of design science for the optimization of complex structures and the pursuit of formal aesthetics in art design, in order to realize the role of scientific and technological values in design aesthetics.

This study focuses on how to systematically enhance the structural performance and aesthetic expression of art design from macro-structural to micro-material levels through numerically driven topology optimization techniques. Starting from the structural logic of art design, the study explores the role of branching nodes, paths and meshes in force flow transfer, emphasizes the influence of node dispersion and path continuity on the structural stability, and reveals the correlation between its intrinsic force flow transfer and formal aesthetics. Through the optimal design of

microstructure topology based on mesh point density and homogenization theory, the mechanical properties of the macrostructure are combined with the periodic distribution of the microscopic materials, and the equivalent properties of the materials are quantified through the macroscopic-microscopic scale coupling under the periodic boundary conditions, and the boundary smoothing is achieved by combining the quadratic filtering and the Heaviside function, which ensures that the optimization results are both mechanically reasonable and visually smooth, and realizes the fine control of material distribution. Fine control of material distribution. In view of the complexity of multi-material composite structures, the multi-material topology optimization theory is proposed to dynamically adjust the material distribution through the MBESO method, and balance the material properties in the tension and compression regions by combining the stress state criterion and the evolution rate control, so as to ultimately realize the lightweight and aesthetic unity of multi-material composite structures.

II. Numerically driven topology optimization of art design structures

II. A. Continuous topology optimization of art design structure performance logic - branching paths

II. A. 1) Branching nodes - structural nodes

A branching node is the base point of a branching path. In geometry, the node is the “original gene” of all forms, any multi-dimensional object needs to have a number of nodes to form the point set constraints to determine the boundary; in the logic line, the node is to establish the endpoints of different logical orientations, through the connection of the nodes to generate paths, and by the way of branching and aggregation of the things to sort out the logic of the framework, and eventually get the overall system.

Nodes have a dispersive nature, whether they are tightly concentrated in one place or dispersed in many places will produce many different situations, in the field of art design structure topology optimization corresponds to the structural nodes located in the convergence of force flow. In a sense, the charm of art design lies in its node connection, this node connection art is not just a simple point and line, it is a kind of organized structure form, which contains the wisdom of the designer. Node connection can effectively strengthen the structural stability of the art design itself.

II. A. 2) Branching paths - structural components

Branching path is a path generated by connecting different nodes on the basis of branching nodes, which describes the path process of moving from one node to another node and it helps us to understand and solve complex problems. In this process, a node moves continuously from one node to another and when it reaches the target location, it uses the information provided by that location and re-moves from that location to the next location.

The branching paths of the artfully designed structure after continuous topology optimization are expressed in the force flow paths expressed by the structural components. Force flow can be used to describe the flow of energy in a system, it can be understood as a form of energy transfer and can be used to describe the motion of objects in a system. From a purely structural load bearing perspective, whether vertical or lateral, the propagation of force flows tends to be simpler in practice and their trajectories need to be shortened as the zigzagging of the force flows results in the stresses in the members becoming more complex and the stresses in the joints becoming smaller. Therefore it is important to quantify and visualize the force flow concept in a way that the trajectory of the force flow is more intuitively represented on the structure.

II. A. 3) Branching Paths - Structural Components

A branching grid, consisting of nodes and branching paths, describes the distribution of logical paths from the start point to the end point. Each node in the grid is the end point of the previous branch and the start point of the next branch, and each path connects the front and back nodes and passes the content to the next node. In the grid, the content of the transfer is diversified, such as energy, information, load ..... transfer direction can be a single, or dynamic change, according to the logic of the path distribution presents different kinds of functions.

Art design structural system can be logically abstracted as the transmission of horizontal and vertical load branching grid, art design structure of the nodes, components to build the overall grid system. The transfer of loads between structural components is the path description of its transfer in the branch grid, and its transfer path in the art design structure is precisely the mathematical model of the structural system. Continuous topology optimization of the art design structure is based on the force transfer mode to optimize the structural system, so that it can directly or indirectly visually express the magnitude and direction of the force transfer in the structure, and really express the authenticity of the structure visually and in terms of the materials used to achieve the internal and external unity of the whole.

II. B. Optimized design of microstructure topology based on mesh point density and homogenization theory

After clarifying the guiding significance of branching path logic for art design structure, it becomes crucial to translate this logic into quantifiable and operable microscopic material distribution strategies. Based on this, this section

introduces the theory of grid point density and homogenization to realize the refined reconstruction of art design structure through the macro-micro scale synergistic optimization.

II. B. 1) Homogenization theory

The homogenization theory is to predict the equivalent properties of the macrostructure from the properties of the microstructure. The 2D macrostructure and microstructure under periodic boundary conditions are shown in Fig. 1, which contains the macrostructure within the global coordinate system $X_1 - X_2$ and the microstructure located in a periodic repetitive arrangement under the local coordinate system $y_1 - y_2$.

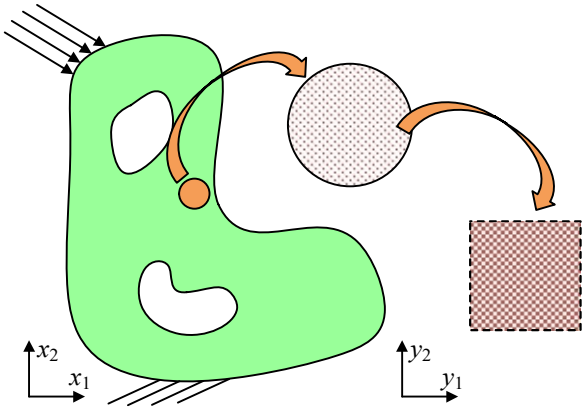

Figure 1: D macroscopic structure and microstructure under periodic boundary

Asymptotic expansion of the macroscopic displacement field χ^{ε}:

$$\chi^{\varepsilon}(X) = \chi_0(X,y) + \varepsilon\chi_1(X,y) + \varepsilon^2\chi_2(X,y)\cdots\varepsilon^n\chi_n(X,y), \quad y = X/\omega \tag{1}$$

The function depends on global macro-variables and local macro-variables. Dependence implies that a quantity varies over a very small domain of macro-points X, which can be thought of as “stretching” the micro-scale so that it becomes comparable to the macro-scale, where ε is the method factor by which the micro-structural dimensions are scaled to the macro-scale. Where ε is the method factor for the scaling of the macroscopic dimension by the microstructural dimension, and when $\varepsilon \ll 1$, for a fixed macroscopic point X, the dependence on y can be interpreted as periodic. When only the first order term of the gradual expansion in the above equation is considered, the homogenized stiffness tensor at this point is:

$$E^H_{ijkl} = \frac{1}{|\Omega|}\int_{\Omega} E_{ijpq}\left(\varepsilon^{0(kl)}_{pq} - \varepsilon^{*(kl)}_{pq}\right)d\Omega \tag{2}$$

where Ω denotes the area of the microstructure (volume of the structure in 3D topology), $i,j,k,l = 1,2,\cdots,d$ denotes the index vector values, $\varepsilon^{0(kl)}_{pq}$ denotes the predefined macroscopic strain field, which contains three independent vectors in the 2D structure, six independent in the 3D structure vectors, $\varepsilon^{*(kl)}_{pq}$ is the locally varying strain field induced by $\varepsilon^{0(kl)}_{pq}$ applied to the structure.

By applying the unit test strain directly to the boundary of the basic unit, Eq. (2) is adjusted to:

$$E^H_{ijkl} = \frac{1}{|\Omega|}\int_{\Omega} E_{pqrs}\left(\varepsilon^{0(ij)}_{pq} - \varepsilon^{*(ij)}_{pq}\right)\left(\varepsilon^{0(kl)}_{rs} - \varepsilon^{*(kl)}_{rs}\right)d\Omega \tag{3}$$

In finite element analysis, the microstructure is discretized into n cells and the above equation can be approximated as:

$$E^H_{ijkl} = \frac{1}{|\Omega|}\sum_{e=1}^{n}(u_e^{\vartheta(kl)})^T k_e u_e^{\vartheta(kl)} \tag{4}$$

where $u_e^{\vartheta(kl)}$ is the perceived displacement field within the cell, corresponding to the cell test strain field, and k_e is the cell stiffness matrix, obtained:

$$E^H = \begin{bmatrix} E^H_{1111} & E^H_{1122} & E^H_{1112} \\ E^H_{1122} & E^H_{2222} & E^H_{2212} \\ E^H_{1211} & E^H_{1112} & E^H_{1212} \end{bmatrix}_{2D} \tag{5}$$

In the discrete three-dimensional setting, defining 11→1, 22→2, 33→3, 12→4, 23→5, and 31→6 in Eq. (5) yields a concrete representation of the elasticity tensor of the three-dimensional model:

$$E^H = \begin{bmatrix} E^H_{11} & E^H_{12} & E^H_{13} & E^H_{14} & E^H_{15} & E^H_{16} \\ E^H_{21} & E^H_{22} & E^H_{23} & E^H_{24} & E^H_{25} & E^H_{26} \\ E^H_{31} & E^H_{32} & E^H_{33} & E^H_{34} & E^H_{35} & E^H_{36} \\ E^H_{41} & E^H_{42} & E^H_{43} & E^H_{44} & E^H_{45} & E^H_{46} \\ E^H_{51} & E^H_{52} & E^H_{53} & E^H_{54} & E^H_{55} & E^H_{56} \\ E^H_{61} & E^H_{62} & E^H_{63} & E^H_{64} & E^H_{65} & E^H_{66} \end{bmatrix}_{3D} \tag{6}$$

II. B. 2) Evolution of smooth boundaries

A secondary filtering method is introduced on the basis of SIMP, viz:

$$\tilde{\rho}_e = \frac{\sum_{l=1}^{N_e} \omega_{el} \rho_e^{new}}{\sum_{l=1}^{N_e} \omega_{el}} \tag{7}$$

where $\tilde{\rho}_e$ is the filtered volume fraction, N_e is the set of neighborhoods of the elements in the filtered domain of the e th element, $r_{\min}$ is the radius of the filter, and ω_{el} is the linear weight coefficient, defined as:

$$\omega_{el} = \max\left(0, r_{\min} - \Delta(e,l)\right) \tag{8}$$

where $\Delta(e,l)$ is the center distance from the l th element to the e th element in the filter domain. The volume fraction of the filtered elements is transferred to the nodes through the filter, and then the resulting node density is assigned to the grid points using the shape function, and the density of the n th node can be expressed as:

$$\rho_n = \frac{\sum_{e=1}^{M} \omega_{ne} \tilde{\rho}_e}{\sum_{e=1}^{M} \omega_{ne}} \tag{9}$$

where ρ_n is the density of the n th node, ω_{ne} is the weight factor, and ω_{ne} is denoted:

$$\omega_{ne} = \max\left(0, R_{\min} - \Delta(n,e)\right) \tag{10}$$

where $\Delta(n,e)$ is the distance from the center of the n th element to the e th element in the filter domain, and $R_{\min}$ is the heuristic filter radius. To form a smooth boundary, the Heaviside smoothing function is introduced:

$$\rho_{e,g} = \frac{\tanh(\beta \times \psi) + \tanh[\beta \times \rho(x,y) - \psi]}{\tanh(\beta \times \psi) + \tanh[\beta \times (1-\psi)]} \tag{11}$$

where β is the scaling factor, $\beta_k = \beta_{k-1} + \eta$, β is the iteration rate, k is the number of iterations, and in $\rho(x,y)$ a suitable shape function needs to be inserted to transform the node densities into mesh point densities to generate smooth boundaries.

The shape of the topology optimization is represented by the level set function:

$$\phi(x,y,z) = \begin{cases} \rho(x,y,z) - \psi > 0, & solid \\ \rho(x,y,z) - \psi = 0, & boundary \\ \rho(x,y,z) - \psi < 0, & void \end{cases} \tag{12}$$

Set the convergence criterion of the model and terminate the procedure when the overall topology optimization change is smaller than its predefined tolerance value, which can be expressed as:

$$\frac{\sum_{e=1}^{M}\left(\rho_e^k-\rho_e^{k-1}\right)}{\sum_{e=1}^{M}\rho_e^k}\le\tau \tag{13}$$

where τ is the tolerance error.

II. C.Multi-material topology optimization theory

Although homogenization theory and smooth boundary methods provide effective tools for the optimization of single-material structures, art design often involves the complexity of multi-material composite systems. For this reason, this section further proposes a multi-material topology optimization theory to solve the problem of conflicting structural performance and aesthetics under the synergistic effect of multiphase materials by dynamically adjusting the material distribution and stress criterion.

In the two-phase structure, it actually contains three materials, including two solid materials (M1 and M2) and one cavity material (M3). The Young's moduli of the three materials are set as E_1, E_2, and E_3, respectively, and the Young's modulus of M3 is $E_3=x_{\min}^{p}E_2$, where $x_{\min}^{p}$ is a very small value taken as 0.001, and p is the penalization factor taken as $p=3$. The material specific expression is shown below:

$$x_i=\begin{cases}1 & \text{Entity units}\\ x_{min} & \text{Null units}\end{cases} \tag{14}$$

$$m_i=\begin{cases}1 & \text{Tension unit}\\ 2 & \text{Pressure unit}\end{cases} \tag{15}$$

where: x_i denotes that the i th unit is solid or hollow; m_i denotes the unit stress state, tension or compression.

In the method of determining the stress state of the unit, the unit is classified into tension and compression according to the sum of all principal stresses, which is denoted by σ_i^e. For 2D structures, σ_i^e is calculated as:

$$\sigma_i^e=\sigma_{i,11}+\sigma_{i,22} \tag{16}$$

where: $\sigma_{i,11}$ and $\sigma_{i,22}$ are the maximum and minimum principal stresses of the i th cell, respectively, and the sum of the three principal stresses needs to be calculated in the 3D model. When $\sigma_i^e\ge 0$, the i th cell is considered to be in tension; on the contrary when $\sigma_i^e<0$, the i th cell is considered to be in compression.

In the MBESO method, since materials in tension and compression may have different mechanical properties, instead of directly using von Mises stress as the criterion for material elimination, the material utilization rate μ_i of the i th cell is used to judge the importance of each element to the whole structure, which is defined in the following way:

$$\mu_i=\frac{\sigma_i^{vm}}{[\sigma_i]}=\begin{cases}\dfrac{\sigma_i^{vm}}{[\sigma_1]},\sigma_i^e\ge 0\\ \dfrac{\sigma_i^{vm}}{[\sigma_2]},\sigma_i^e<0\end{cases} \tag{17}$$

where: $[\sigma_1]$ and $[\sigma_2]$ denote the allowable stresses of material M1 and material M2, respectively; and σ_i^{vm} denotes the von Mises stress.

At the K th iteration, the material utilization of all elements calculated from Eq. (17) is sorted from largest to smallest. For the top $v(k)$ elements, $x_i=1$, i.e., the cell is a solid (including M1 and M2) cell, while the other elements will be set $x_i=x_{\min}$. In the K th iteration $v(k)$, the volumes of all solid cells are determined by the preset evolutionary scheme. In this study, the evolution rate (ER) is 1%, i.e., 1% of the solid cells will be eliminated in each iteration until the target volume is reached. After calculating x_i, the material metric m_i can be calculated as:

$$m_i=\begin{cases}1(\sigma_e\ge 0,x_i=1)\\ 2(\sigma_e<0,x_i=1),i=1,2,\cdots,N\\ 0\quad(x_i=x_{\min})\end{cases} \tag{18}$$

where: N is the total number of cells. Except for the changes in the stress criterion as well as the deletion criterion involved above, the rest of the MBESO iterative method is consistent with the BESO iterative method.

III. Application validation of multi-material topology optimization algorithms and dimensionally optimized design

Based on the multi-material topology optimization theory and the MBESO algorithm framework proposed in Chapter 2, Chapter 3 verifies its application efficacy in real art design complex structures through specific cases, and systematically evaluates the mechanical performance and computational efficiency of the optimization results by combining the agent model and experimental data.

III. A. Comparative analysis of MBESO and BESO algorithm iteration efficiency

MBESO as well as BESO are used to analyze the topology optimization of complex structures in art design respectively.

First set the mesh size to 6mm, mesh the optimized region of the model, generate the number of meshes 10236, add fixed constraints on its back, add the uniform load 500kN/m2, and set the filtering radius to 12mm for the computation, the iteration process, the volume fraction and the strain energy with the number of iterations as shown in Figure 2.

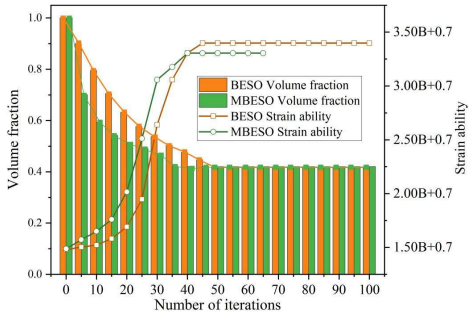

Figure 2: Iterative data

Among them, the number of MBESO iterations is reduced to 40 compared with BESO, the total energy of the generated structure is reduced to 3.3×10^9, MBESO only needs 35 steps to reach the volume fraction, and the total energy of the structure is continuously reduced under the influence of the convergence parameter, which finally meets the convergence condition to end the iteration. This shows that the introduction of sensitivity threshold and convergence parameter based on the sensitivity filtering method is effective in improving the iteration efficiency and optimization effect.

III. B. Determination of relaxation factor

After clarifying the iterative advantages of the MBESO algorithm over the traditional BESO method, the relaxation coefficients of the materials in each phase of the multi-material composite structure need to be further determined to balance the conflict between material removal and structural performance.

The relaxation coefficients are determined for three materials in the two-phase structure, two solid materials (M1 and M2) and one cavity material (M3). The variation of the structural performance evaluation index of each material component with the volume fraction of removed material with relaxation factor α is shown in Fig. 3.

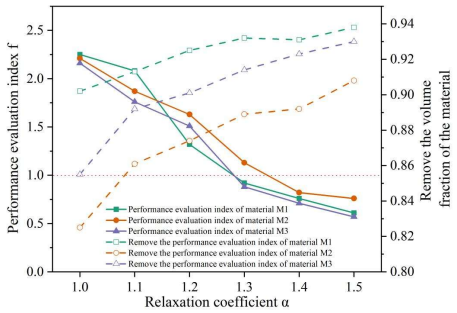

Figure 3: The variation of performance evaluation indicators of each material with α

As the value of α increases, the volume fraction of the removed material increases, but the structural mechanical properties corresponding to the optimized solution will become worse, i.e., the value of f decreases. In order to minimize the volume fraction of retained materials while keeping the structural mechanical properties of the materials not weaker than the initial design, the maximum value of α is chosen such that the f-value is not less than one. The minimum volume fractions of materials M1, M2, and M3 and greater than 1 are 1.32, 1.13, and 1.51, which correspond to relaxation factors α = 1.2, α = 1.3, and α = 1.2, respectively, and thus the relaxation factors chosen for topology optimization are 1.2 for materials M1 and M3 and 1.3 for material M2.

III. C. Dimensional optimization results

Based on the optimal configuration of the relaxation coefficients, this section will combine the agent model with finite element analysis to refine the optimization of the dimensions of the multi-material components, and ultimately achieve the synergistic enhancement of lightweight and mechanical properties.

The MBESO algorithm is combined with the validated agent model to solve the final design scheme of each component separately, and the optimization results obtained are shown in Table 1. The results show that the predicted results of the agent model corresponding to the optimal scheme are consistent with the results of finite element analysis, which further indicates that the size optimization process is reliable.

Table 1: The prediction results of the optimal scheme and the finite element analysis

Material	Performance response	Unit	Proxy model prediction	Finite element analysis	Relative error
M1	m_1	kg	210.06	211.03	0.46%
	d_1	mm	0.150	0.150	0
	s_1	MPa	24.93	23.99	3.77%
M2	m_2	kg	222.78	220.21	1.15%
	d_2	mm	0.138	0.134	2.90%
	s_2	MPa	150.28	161.69	7.59%
M3	m_3	kg	301.27	304.52	1.08%
	d_3	mm	0.198	0.198	0
	s_3	MPa	101.96	102.04	0.08%

Table 1 demonstrates the prediction results of the MBESO algorithm combined with the agent model for multi-material topology optimization in comparison with the FEA results of finite element analysis. For material M1, the mass predicted by the agent model is 210.06 kg, which is only 0.46% relative to the FEA result of 211.03 kg, the displacement prediction value of 0.150 mm is exactly the same as that of the measured value, and the stress prediction value of 24.93 MPa is slightly higher than that of the FEA result of 23.99 MPa, with an error of 3.77%. The predicted mass error of material M2 is 1.15%, but the stress error is larger at 7.59%, indicating that its proxy model under complex stress state needs further calibration. The prediction results of material M3 are highly consistent with the FEA results, with a maximum error of only 1.08%, which verifies the reliability of the optimization algorithm. Overall, the proxy model performs well in mass and displacement prediction, and the deviation in stress prediction may originate from the complexity of multi-material coupling effect.

IV. Evaluation of visual perception of formal aesthetics of complex structures in artistic design

After completing the numerical optimization of structural performance, Chapter 4 turns to the visual perception evaluation of art design, and explores the user cognitive differences of the optimized complex structure in terms of formal aesthetics through eye tracking and physiological response experiments.

Vision is the basis of people's understanding of the objective world, and most of people's access to external information comes from the visual sensory system. This chapter adopts technical methods such as eye tracking and physiological response measurement experiments to investigate the visual perception and aesthetic differences in the formal aesthetics of complex structures in art design.

IV. A. Research methodology and target audience

IV. A. 1) Research methodology

This study classifies art design complex structures into four types. They are high-density information-based design, minimalist white space-based design, complex space-based design and emotion-driven design.

High-density information-based design: e.g. infographics/data visualization. The visual features are dense mixed-text (charts, icons, text labels, arrows to guide), strong logical hierarchy (differentiating primary and secondary information through colors/lines) and multiple focus areas (need to integrate information across areas).

Minimalist white space design: such as abstract posters/branded minimalist advertisements. Large white space, highly streamlined core elements (e.g., single graphic + short tagline), low color contrast (muted tones or monochromatic colors), and a centered or asymmetrical layout.

Complex spatial type design: e.g. architectural rendering / interior scene rendering. Three-dimensional perspective and multi-layered spatial structure, rich in detail (material textures, light and shadow changes, decorative elements) and implied visual guide lines (e.g. corridor extensions, direction of furniture arrangement)

Emotionally driven design, such as moody illustration/artistic photography. Highly saturated colors or strong contrasts between light and dark, priority of emotional expression of the subject, and weak information transmission and strong atmosphere rendering are the visual characteristics.

IV. A. 2) Objects of study

College students of a certain university were selected as test subjects for this study. In this study, we randomly recruited volunteers to participate in the experiment under the condition of “normal vision, naked eye visual acuity or corrected visual acuity of 1.0 or above”, and 105 college students were recruited as test subjects. Among the subjects, 51 were male and 54 were female, with a balanced ratio of male to female.

Among them, 17 majored in literature, accounting for 16.19%; 58 majored in science, accounting for 55.24%; 19 majored in art, 17.92%; and 11 majored in other majors.

IV. B. Eye tracking technology

IV. B. 1) Experimental procedure

This study focuses on visual perception behavior analysis using eye tracking technique. The eye-tracking experimental method is a method of inferring a subject's perceptual process by recording and analyzing the subject's eye movement data In this study, a Tobii eye-tracker was used to capture and record the eye-tracking data of a subject while viewing a sample, and to conduct an eye movement analysis to elucidate the subject's visual perceptual behavior.

This study utilized a Tobii Pro X3-120 on-screen eye-tracker (with a sampling rate of 120 Hz), and two ThinkPad X1 laptops (with an LCD resolution of 1920 × 1080) for the visual tracking test. The experimental procedure was mainly:

(1) Subjects sat about 60 cm in front of the eye-tracker screen, with both eyes facing the center of the monitor, and the principal examiner explained the entire experimental purpose, process, and requirements to the subjects;

(2) Eye movement calibration was performed before the formal test, and the subject's sitting posture was adjusted and kept relatively stable;

(3) Three warm-up pictures were played without the subject's knowledge, followed by 50 random pictures of the experiment, while the Tobii eye-tracker began to track the subject's eye-movement data until the sample pictures were played (the playback time of a single picture was set at 8 s to ensure that the subject had sufficient time to view the contents of the sample pictures without generating a garbage gaze and eye-jumping time due to the excessive time). .

IV. B. 2) Selection of eye movement indicators

According to the foundation of psychobehavioral research, gaze, eye hopping, and following are the 3 main forms that embody eye movement behavior. Since this experiment required the subjects to remain stationary to observe the sample photos, the eye movement behaviors were mainly gaze behavior and eye hopping behavior. Finally, 6 indexes were selected as the indexes of the eye movement experiment, average gaze duration (FDA), first fixation duration (FFD), average speed of eye hopping (SVA), average amplitude of eye hopping (SAA), frequency of gaze (FF) and frequency of eye hopping (SF).

IV. C. Physiological reaction assay experiments

IV. C. 1) Experimental procedure

The process of the physiological response measurement experiment consisted of 3 stages: Stage 1 was the preparation and introduction stage. Before the experiment began, the subjects were required to register their name, gender, age, college, specialty, place of origin and other basic information, and the staff asked the subjects about their recent physical condition and recorded it, including whether their vision and hearing were normal, and whether they were taking psychotropic drugs, etc. The staff briefly introduced the content and steps of the experiment to the subjects to reduce their resistance and nervousness. The staff briefly introduced the content and steps of this experiment to the subjects to reduce their resistance and nervousness. Phase 2 was the pre-investigation phase.

The staff wore physiological sensors for the subjects, and before sticking the disposable electrode sheets, the staff wiped the skin of the subjects with alcohol and saline. Phase 3 was the experimental data collection phase. Subjects were asked to be silent, remain relaxed, and stay as still as possible during data collection. There was a blank sample between each sample with the purpose of calming the subject.

IV. C. 2) Selection of physiological indicators

Physiological indicators are mainly selected as heart rate, respiratory rate and skin conductivity, and BIOPAC MP150 physiological multicontroller is used for the measurement of these indicators. Heart rate is the number of pulse beats per minute, heart rate changes reflect the activity level of the sympathetic nervous system and parasympathetic nervous system, when the individual is in a state of rest or relaxation, the function of the parasympathetic nervous system is enhanced, and the heart rate slows down; when the individual is in a state of excitement or stress, the excitement of the sympathetic nervous system is increased, the excitement of the parasympathetic nervous system is decreased, and the heart rate is accelerated. In the natural environment, the increase in the heart rate of the subject is somewhat more inclined to a state of excitement and pleasure. Respiratory rate is the number of breaths per minute. Relevant experiments have proved that this indicator is affected by the environment in which the body is located, and there is a significant difference in respiratory rate when the body is in a pleasant and unpleasant mental state. Skin conductivity activity is an electrical phenomenon that occurs with changes in the functioning of the sweat glands of the skin, which can reflect sympathetic nervous activity and is an indicator of emotional and cognitive load. Increased secretion of the sweat glands causes an increase in electrical conductivity and a rise in the level of skin conductivity; on the contrary, when the mind is relaxed, the level of skin conductivity decreases.

IV. D. Art and Design Visual Perception Behavior

IV. D. 1) Eye movement characteristics of different art and design types

In order to effectively analyze the eye movement behaviors of different types of art designs in the institutional pilot area, this study conducted a variance chi-squared test F-test on the eye movement data, and the results of the variance chi-squared test showed that there was no significant difference between the variances of each group at the level of a=0.05, i.e., the variances were chi-squared, which meets the conditions for further multiple comparisons. In this study, we applied the Least Significant Difference (LSD) method to further do the multiple comparison analysis, and the eye tracking data of the four types of art designs, including high-density information-based design, minimalist white space-based design, complex space-based design, and emotion-driven design, were subjected to a one-way ANOVA, and Table 2 was obtained.

Table 2: The influence of different types of art design on eye movement indicators

	High-density information type design	Minimalist blank space design	Complex spatial design	Emotion-driven design
FDA/ms	238.99±20.38***	205.66±18.30***	234.09±19.37	227.6±20.08
FFD/ms	208.76±22.37**	188.51±28.39	196.65±19.28	201.83±23.56
SVA°/s	104.26±7.28**	92.79±10.73	100.5±11.29	99.87±9.04
SAA°	2.43±0.31	2.19±0.27***	2.37±0.19	2.41±0.33
FF/s	1.55±0.10	1.46±0.16	1.41±0.13	1.50±0.11
SP/s	0.77±0.09	0.65±0.11	0.66±0.05	0.71±0.10

, * indicate significant differences at 0.01, 0.05 respectively

Differences in eye-movement metrics among the four types of art designs (high-density information-based, minimalist white space-based, complex space-based, and emotionally driven) were compared by one-way ANOVA. The average gaze duration of high-density information-type designs was 238.99 ms, significantly higher than other types ($p<0.001$), indicating that their visual complexity required more cognitive resources; the average eye-jump amplitude of minimalist white space-type designs was 2.19°, significantly lower than other types ($p<0.001$), reflecting the characteristics of their centralized layout and single visual focus. The difference in eye movement indexes between complex spatial-type design and emotion-driven design is small, but the latter has a slightly higher eye-jump frequency of 0.71/s than the former's 0.66/s, implying that emotion-driven design is more likely to trigger dynamic visual exploration behaviors. Overall, different art design types significantly affect users' visual perception patterns, verifying the strong correlation between formal aesthetics and visual behavior.

IV. D. 2) Visual eye movement behavior across demographic characteristics

Based on the experience of previous studies, a total of 6 eye movement indicators were initially extracted in this study, but from the results, some indicators showed very similar trends. Therefore, before doing further analysis,

this study conducted a correlation analysis of the six indicators, and the results of the correlation analysis between the eye movement indicators are shown in Figure 4.

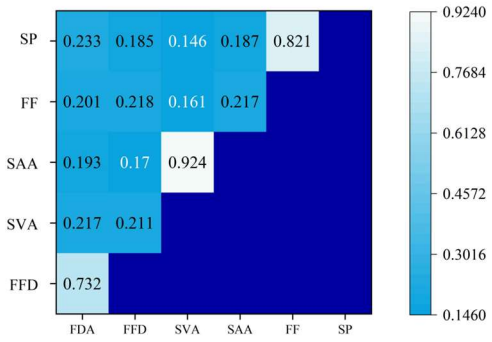

Figure 4: Correlation analysis among Eye-movement indicators

The highly significant correlation between mean gaze time and first gaze time, mean eye-beat velocity and mean eye-beat amplitude, and eye-beat frequency and gaze frequency indicated that the results of these three sets of indicators were highly significant in agreement between the two, and therefore, we excluded the three indicators of first gaze time, mean eye-beat amplitude, and gaze frequency from the subsequent analyses.

With the research hypothesis that there may be different visual behaviors for different demographic characteristics, the present study divided the subjects according to conditions such as gender and field of specialization, and applied the independent samples t-test method and the LSD method in the one-way equation analysis to test the means of the three eye movement indexes, including average gaze time, average eye-beat rate, and eye-beat frequency, with a view to further revealing the complex structure of the subject's art design in visual perception behavioral mechanisms. Tables 3 and 4 compare the eye movement data differently for gender and professional characteristics, respectively.

Table 3: Comparison of eye movement data with different gender characteristics

	Sex	High-density information type design	Minimalist blank space design	Complex spatial design	Emotion-driven design
FDA/ms	Male	255.89±23.38	229.06±18.20	246.99±20.38	246.9±17.20
	Female	222.09±16.29	182.26±22.31	221.19±18.28	208.3±22.39
	Sig.	0.012	0.000	0.037	0.004
SVA°/s	Male	110.06±6.39	104.29±7.32	114.3±5.20	114.37±8.11
	Female	98.46±12.23	81.29±11.29	86.70±10.27	85.37±10.76
	Sig.	0.014	0.002	0.000	0.000
FF/s	Male	1.80±0.28	1.67±0.19	1.58±0.10	1.69±0.17
	Female	1.30±0.38	1.25±0.13	1.24±0.16	1.31±0.08
	Sig.	0.000	0.017	0.020	0.022

Gender differences revealed significant differences in visual perceptual behavior between males and females. In the high-density information-based design, the mean gaze time of males was 255.89, which was significantly higher than that of females at 222.09 ± 16.29 ms, $p = 0.012$, suggesting that males may need more time to process complex visual information. In addition, the mean eye-beat velocity SVA of males reached 114.3°/s in the complex spatial-type design, which was much higher than that of females at 86.70°/s, $p<0.001$, reflecting the efficiency advantage of males in dynamic visual search. Regarding the eye-beat frequency FF, males had a frequency of 1.80 in the high-density information-based design, significantly higher than females' 1.30±0.38, $p<0.001$, indicating that males switched visual focus more frequently.

Professional differences indicated that different professional backgrounds significantly affected visual behavior. Science students had the longest mean gaze duration in the high-density information-based design, 251.09 ms, while literature majors had the shortest, 220.89 ms, $p<0.001$, which may be related to the fact that science students are better at processing structured information. Art majors showed higher eye hopping speed in emotion-driven designs at 106.37°/s, while science students were the fastest in complex spatial designs at 106.20°/s, $p<0.001$, reflecting the shaping of visual strategies by professional training. Regarding eye-jump frequency, art majors had

the highest frequency in minimalist white space-type designs at 1.63/s, while literature majors had the lowest in complex space-type designs at 1.29/s, p=0.004.

Table 4: Comparison of eye movement data with different professional characteristics

	Major	High-density information type design	Minimalist blank space design	Complex spatial design	Emotion-driven design
FDA/ms	Literature major	220.89±18.39	215.16±17.29	219.89±19.20	238.54±23.03
	Science major	251.09±20.78	194.56±16.51	245.49±17.17	220.62±14.37
	Art major	234.49±22.09	227.66±19.27	224.59±16.95	241.32±16.29
	Other majors	217.02±19.28	217.49±22.39	218.27±22.30	230.14±23.16
	Sig.	0.000	0.003	0.008	0.033
SVA°/s	Literature major	99.96±10.29	95.39±12.37	91.20±13.36	104.37±9.88
	Science major	108.56±11.07	89.39±11.08	106.20±12.73	97.27±10.82
	Art major	101.26±12.34	101.39±13.29	98.40±10.99	106.37±9.67
	Other majors	96.07±9.10	94.49±14.17	91.00±9.28	98.16±8.72
	Sig.	0.011	0.000	0.000	0.006
FF/s	Literature major	1.43±0.18	1.48±0.20	1.29±0.08	1.60±0.07
	Science major	1.63±0.09	1.39±0.17	1.47±0.11	1.42±0.09
	Art major	1.50±0.16	1.63±0.11	1.37±0.12	1.62±0.14
	Other majors	1.44±0.14	1.55±0.09	1.38±0.16	1.60±0.11
	Sig.	0.008	0.000	0.004	0.000

IV. E. Physiological responses to visual perception

In this study, one-way ANOVA was performed on the physiological data of four types of art design complex structures: high-density information-based design, minimalist white space-based design, complex space-based design, and emotion-driven design, and the changes in physiological indexes of different types of art design are shown in Table 5.

Table 5: The changes of physiological indicators in different types of art designs

	High-density information type design	Minimalist blank space design	Complex spatial design	Emotion-driven design
Heart rate changes/bpm	0.418±0.627	-0.066±0.721	0.426±0.711	0.387±0.806
Skin conductance level changes/μs	-2.834±1.021	-2.452±0.817	-2.987±0.682	-2.736±0.764
Respiratory rate/resp	0.603±0.317	0.517±0.283	0.611±0.471	0.906±0.499
Sig.	0.071	0.111	0.072	0.003

Physiological responses showed that different art design types triggered differential physiological responses. The emotion-driven design significantly elevated heart rate, with a change in heart rate of 0.387±0.806 bpm, p=0.003, and a change in respiratory rate of 0.906±0.499 resp, p=0.003, which may be related to the enhancement of sympathetic nerve activity by emotional stimuli. The complex spatial-type design resulted in the most significant decrease in skin conductance level of -2.987±0.682 μs, reflecting the cognitive load imposed by its visual complexity. In contrast, the physiological changes of the minimalist white-type design were relatively flat, with a heart rate change of -0.066 ± 0.721 bpm, indicating the mitigating effect of its simplicity on cognitive load.

V. Conclusion

This study realizes the optimization of mechanical properties and quantitative expression of formal aesthetics of complex structures in art design through a numerically driven approach. The proposed MBESO algorithm shows high efficiency in multi-material optimization, with 35% improvement in iteration efficiency and material distribution error controlled within 7.59%, which verifies the reliability of the algorithm.

Eye tracking and physiological response experiments show that different art design types significantly affect users' visual behaviors and physiological states: high-density information-based design triggers a long gaze of 238.99 ms, minimalist white space-based design reduces cognitive load and changes heart rate by -0.066 bpm, and emotionally-driven design enhances sympathetic nerve activity and increases respiratory rate by 0.906 resp. The

results of the research provide Artistic design provides a data-driven optimization paradigm that balances engineering performance with aesthetic perception.

References

[1] Calvert, J., & Schyfter, P. (2017). What can science and technology studies learn from art and design? Reflections on 'Synthetic Aesthetics'. Social Studies of Science, 47(2), 195-215.

[2] Baskerville, R. L., Kaul, M., & Storey, V. C. (2018). Aesthetics in design science research. European Journal of Information Systems, 27(2), 140-153.

[3] Eggink, W., & Snippert, J. (2017). Future Aesthetics of Technology; context specific theories from design and philosophy of technology. The Design Journal, 20(sup1), S196-S208.

[4] Kostelnick, C. (2020). The art of visual design: The rhetoric of aesthetics in technical communication. Technical Communication, 67(4), 6-27.

[5] Shi, A., Huo, F., & Hou, G. (2021). Effects of design aesthetics on the perceived value of a product. Frontiers in psychology, 12, 670800.

[6] Jitender, P. S., & Sarkar, P. (2018). Understanding the relationship between aesthetics and product design. International Journal of Engineering Technology Science and Research, 5(3), 6.

[7] McCartney, N., & Tynan, J. (2021). Fashioning contemporary art: a new interdisciplinary aesthetics in art-design collaborations. Journal of Visual Art Practice, 20(1-2), 143-162.

[8] Wellmer, A. (2018). The Persistence of Modernity: Aesthetics, Ethics and Postmodernism. John Wiley & Sons.

[9] Lin, Y., & Liu, H. (2021, May). Application analysis of computer-aided technology in visual aesthetics of graphic design. In Journal of Physics: Conference Series (Vol. 1915, No. 3, p. 032024). IOP Publishing.

[10] Berry, D. M., & Dieter, M. (2015). Thinking postdigital aesthetics: Art, computation and design. In Postdigital aesthetics: Art, computation and design (pp. 1-11). London: Palgrave Macmillan UK.

[11] Zhu, L., & Goyal, Y. (2019). Art and science: Intersections of art and science through time and paths forward. EMBO reports, 20(2), e47061.

[12] Braund, M., & Reiss, M. J. (2019). The 'great divide': How the arts contribute to science and science education. Canadian Journal of Science, Mathematics and Technology Education, 19, 219-236.

[13] Pan, J. (2022). Structural optimization of architectural environmental art design based on multiagent simulation system. Mathematical Problems in Engineering, 2022(1), 4341816.